IEEE Computer Society Conference on Computer Vision and Pattern Recognition, June 2007

Inferring Grammar-based Structure Models from 3D Microscopy Data

Joseph Schlecht[†] Kobus Barnard[†] Ekaterina Spriggs[†] Barry Pryor[‡]

[†]Computer Science Department
University of Arizona
{schlecht, kobus, taralove}@cs.arizona.edu

[‡]Plant Sciences Department
University of Arizona
bmpryor@u.arizona.edu

Abstract

We present a new method to fit grammar-based stochastic models for biological structure to stacks of microscopic images captured at incremental focal lengths. Providing the ability to quantitatively represent structure and automatically fit it to image data enables important biological research. We consider the case where individuals can be represented as an instance of a stochastic grammar, similar to L-systems used in graphics to produce realistic plant models. In particular, we construct a stochastic grammar of Alternaria*, a genus of fungus, and fit instances of it to microscopic image stacks.*

We express the image data as the result of a generative process composed of the underlying probabilistic structure model together with the parameters of the imaging system. Fitting the model then becomes probabilistic inference. For this we create a reversible-jump MCMC sampler to traverse the parameter space. We observe that incorporating spatial structure helps fit the model parts, and that simultaneously fitting the imaging system is also very helpful.

1. Introduction

The function of an object is often closely related to its structural form. As a result, the process of understanding what a novel item *is* or *does* frequently begins with an inspection of its structure. This is particularly true in biology, where scientific inquiries of microscopic specimens focus on observing and quantifying structure in images under varying experimental conditions to test hypotheses of specimen functionality. However, manually obtaining such results is expensive and time-consuming. In this paper we present a new method to automatically infer biological structure from microscopic images using grammar-based models for biological growth.

Many biological structures comprise a set of connected substructures that are recursively related and can be described by a formal set of rules explaining their growth. The set of rules is a grammar for growth and is similar to Lindenmayer-systems [9] used in graphics. By stochastically and recursively applying these rules, an instance of the grammar is generated. We consider such a grammar as a basis for building a probabilistic specimen model to infer from data. The model is constructed so that repeated application of the grammar rules can generate a parameterization of it. Thus, our approach focuses on fitting a complete model of the specimen, unlike previous methods that fit only individual and independent substructures of specimen [1, 13].

Images formed under a transmitted-light microscope contain a significant amount of blur due to the high magnification and shallow depth-of-field in the optics. This makes accurate localization of structure in the images difficult. Rather than try to eliminate the blur from the images through deblurring methods [3, 7], we model the optical system in order to understand the image formation process and unlock structural information captured in the image blur. Combining a grammar-based structure model for a specimen with a model for the optics of the imaging system is an innovative and powerful way to understand microscopic images accurately.

Inferring such models is analytically very difficult; the number of parameters, their interdependence, and the fact that the dimensions of the model is itself a parameter, create a space that is prohibitively complex to work with. Thus, we create a Markov chain Monte Carlo sampler [2, 11] to efficiently explore the parameter space in search of a likely set of parameters that generated the data. The moves of the sampler that guide its search through the model parameter space effectively embody the rules of the grammar for the specimen. Furthermore, the sampler infers both the structure and imaging models simultaneously so that each can benefit from an improved fit of the other. Since the dimensionality of the model is unknown, we further construct a reversible-jump MCMC sampler to handle model selection and traverse the multi-dimensional parameter spaces.

1.1. Scientific motivation

Understanding the morphological structure of an object by modeling it and automatically fitting it to data yields valuable quantitative information that creates further insight into its function. For a biologist interested in analyzing microscopic specimen, automatically inferred structure can be used in a high-throughput data analysis system to improve experimental efficiency and increase the frequency of scientific discoveries. Furthermore, since the function of a specimen is often captured in other modes of data, such as gene expression data, we can couple this with structural information obtained in the fitting process. Multi-model data linking can reveal new functional information that was not previously possible to obtain because of limitations in manual structure quantification. Finally, our model is of the complete structure and, once fit to data, can be used for visualization in virtual environments and three-dimensional printing for tactile exploration.

A good example of a biological specimen whose structure is recursive in nature is *Alternaria*, a microscopic genus of fungus. The general form of *Alternaria* is tree-like with species-dependent branching patterns. It is composed of tubular filaments, hyphae, and ellipsoid-shaped reproductive spores that are darkly pigmented. Species of *Alternaria* are frequently found in soil and organic debris and are estimated to contribute to 25-50% of agricultural spoilage [17]. These species are among the most common potent airborne allergens [16] and one of the most prodigious producers of toxic chemicals, some of which have been linked to forms of cancer [5]. Thus, *Alternaria* is heavily analyzed by mycologists in order to better understand its functionality and discover methods to ameliorate its effects.

To aid in the analysis of *Alternaria* and illustrate our ideas for structure modeling and inference, we developed a grammar-based model for *Alternaria* and sampling methods to fit the model to three-dimensional microscopic images stacks. The image stacks are three-dimensional in the sense that the mycologist who captured them continuously imaged the specimen while increasing the focal length of the microscope. Figure 1 shows images from two of these stacks, A_1 and A_2. Notice the significant blur in the images, a result of the optics in the transmitted-light microscope.

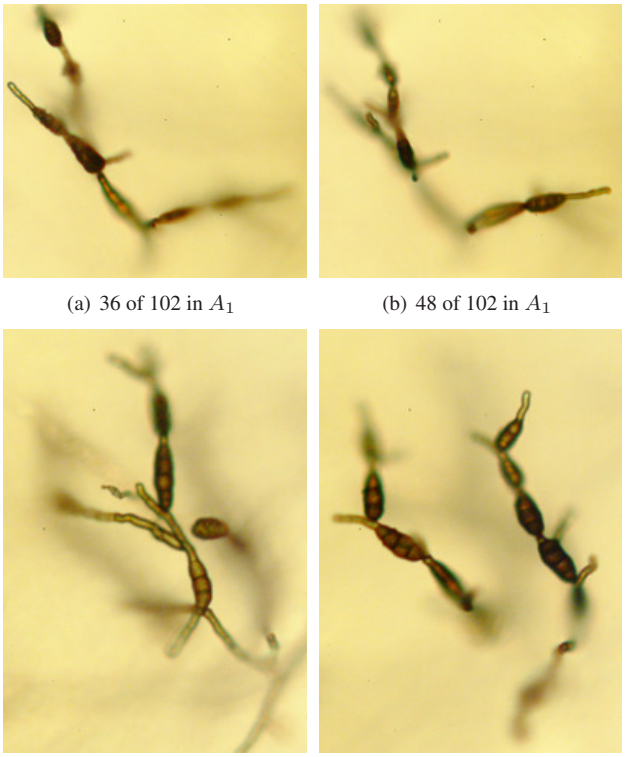

(a) 36 of 102 in A_1 (b) 48 of 102 in A_1

(c) 13 of 82 in A_2 (d) 53 of 82 in A_2

Figure 1. Images from *Alternaria* 3D data sets A_1 and A_2. In each image, the point-spread function of the brightfield transmitted-light microscope generated blur from nearby focal planes.

2. Stochastic grammar for structure

L-systems were invented by the biologist A. Lindenmayer as a mathematical tool to model cellular interactions in plants [8]. L-systems are a type of formal grammar similar to Chomsky grammars with the exception that all rewriting rules are applied in parallel and simultaneously replace all letters in a word [12]. A parametric stochastic context-free L-system is a tuple

$$G_\pi = \langle V, \sigma, \omega, P, \pi \rangle \quad (1)$$

where V is the alphabet, σ is the set of formal parameters, ω is the axiom, consisting of letters from the alphabet, P is a set of production rules, and $\pi : P \rightarrow [0, 1]$ is a probability distribution [12]. Applying the set of production rules to the axiom recursively replaces each letter with other letters from the alphabet, producing a more complex, self-similar structure.

2.1. *Alternaria* L-system

A fungus from the genus *Alternaria* grows similarly to a plant—it has a long vegetative hyphae with branches that have a three-dimensional sporulation pattern [15]. Each branch is a primary conidiophore development which is a type of hypha capable of producing spores. The hyphae cells in a branch can develop another hypha cell through apical growth or a spore from its tip. After a spore develops, several structures can occur, depending on the species: another spore, a lateral intra-conidium hypha branch coming from one cell of the spore, an apical conidium terminus hypha branch, coming from the tip, or a sub-conidium conidiophore hypha branch coming from the hypha cell immediately before the spore.

In general, the fungus produces a new hypha cell or a

spore, which in turn develops more hyphae cells or spores, defining a recursive growth pattern with self-similar structure. To model this growth process we use a parametric, stochastic and context-free L-system.

In our grammar the set of parameters and probability distributions are determined from the morphological characteristics obtained by plant pathologists from observation of the structure. For example, the following rule represents how the long vegetative hyphae grows and develops branches:

$$V\_hypha \rightarrow H(\pi_1, \pi_2, R)\ [\ Branch\ ]V\_hypha \qquad (2)$$

where $H(\pi_1, \pi_2, R)$ represents a number of hyphae cells, obtained from a probability distribution π_1, each cell with length drawn from probability distribution π_2, and each cell at an angle $R(\theta, \phi)$ with respect to the previous structure. A branch is replaced by

$$Branch \rightarrow H(\pi_1, \pi_2, R)\ Cd \qquad (3)$$

where Cd is one of several conidiophore developments - a possible sub-conidium hypha, Cd_3, followed by a spore; or a hypha cell, $h(\pi, R)$; or no change:

$$Cd \rightarrow P_\pi([Cd_3]\ Spore\ Cd_2,\ h(\pi, R)\ Cd,\ Cd) \qquad (4)$$

where P_π represents the probabilities of creating each of the developments.

We complete our grammar for *Alternaria* with the following rules:

$$Cd_2 \rightarrow P_\pi(Spore\ Cd_2,\ Apical\ Cd, \quad Lateral\ Cd,\ Cd_2) \qquad (5)$$

$$Cd_3 \rightarrow P_\pi(h(\pi, R)\ Cd,\ Cd_3) \qquad (6)$$

Figure 2 shows instances generated by this L-system.

To facilitate the process of examining how the parameters define each species, we created an on-line tool which scientists can use to explore a 3D VRML model of the fungus after modifying the parameters and the probability distributions [1].

3. Modeling

Our generative model for 3D microscopic image data of *Alternaria* combines a grammar-based structure representation with a model of the imaging system. This enables us to accommodate the burring effects of the microscope and more accurately infer structure. What follows is a description of each component in our model.

[1] http://vision.cs.arizona.edu/taralove/lsystem.html

(a) 3 iterations (b) 12 iterations

(c) An instance of vegetative hypha with branches

Figure 2. 3D models generated by the L-system, showing growth of simple structures (a), one branch (b), and an instance of the model (c).

3.1. Grammar-based structure

We model the structure of *Alternaria* based on its grammar for growth. We represent its hyphae and spores as an ordered set of ellipsoids and cylinders, and enforce connectedness among these substructures to one apical growth and multiple lateral branches. The model has a root position and direction of growth given by $(\mathbf{p}_r, \varphi_r, \vartheta_r)$, where the position is in the 3D imaging window $\mathcal{W}$. The growth direction is defined by two Euler angles for symmetric objects, *i.e.*, ellipsoids and cylinders. Denote the space containing all root position and orientations by $\mathbb{P}$.

The i^{th} apical hypha with m_h number of branch hyphae is defined as a collection of structure parameters and descendant growth indices.

$$h_i^{(m_h)} = (l, w, \varphi, \vartheta, \lambda, t, j, k_1, \ldots, k_{m_h})\,. \qquad (7)$$

The length and width of the hypha cylinder is l, w; its orientation is given by two Euler angles relative to the growth direction of its apical parent; $\lambda \in [0, 1]$ represents the average opacity of the substructure in the image; and $t \geq 0$ is the integer branch level of the hypha. The index j specifies its apical growth, and the lateral branches are indexed by k.

The spore and branch hypha substructures $s_j^{(m_s)}$ and

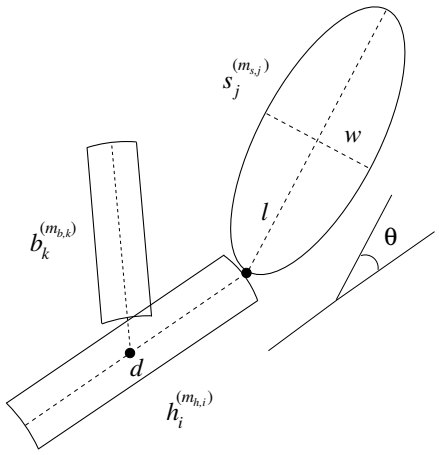

Figure 3. An example of a spore s_j, lateral branch b_k, and apical hypha h_i, and how they are connected in the model of *Alternaria*.

$b_k^{(m_b)}$ are similarly defined (see figure 3). A lateral branch hypha has an additional parameter, $d \in [0, 1]$, specifying the normalized position along the major axis of its parent where the branch is located. The position of all descendant substructures is determined by their size and relative orientation to their parent. The root substructure of the model has a base orientation and position as previously described.

Let $\mathbf{n} = (n_h, n_s, n_b)$ be the number of substructures in the model. Then the number of branch hypha per substructure lies in the space

$$\mathbb{M} = \left\{ \mathbf{M} : \sum_{i=1}^{n_h} m_{h,i} + \sum_{i=1}^{n_s} m_{s,i} + \sum_{i=1}^{n_b} m_{b,i} = n_b \right\}. \quad (8)$$

The parameterization of all ordered sets of n_h apical hypha with $\mathbf{m}_h$ branches is given by

$$\mathbb{H}^{(n_h, \mathbf{m}_h)} = H_1^{(m_{h,1})} \times \cdots \times H_{n_h}^{(m_{h,n_h})}. \quad (9)$$

The parameterizations over all sets of spores and branches are similarly defined as $\mathbb{S}^{(n_s, \mathbf{m}_s)}$ and $\mathbb{B}^{(n_b, \mathbf{m}_b)}$.

By combining the subspaces for root position and orientation, branch hypha distribution, and ordered sets of $\mathbf{n}$ substructures, we define the space over all *Alternaria* models as

$$\Psi^{(\mathbf{n})} = \bigcup_{\mathbf{M} \in \mathbb{M}} \mathbb{P} \times \mathbb{H}^{(n_h, \mathbf{m}_h)} \times \mathbb{S}^{(n_s, \mathbf{m}_s)} \times \mathbb{B}^{(n_b, \mathbf{m}_b)}. \quad (10)$$

The construction of the space is such that an instance of a grammar for *Alternaria* can be mapped into it.

3.2. Imaging system

The image formation process in a microscope is a convolution of the true unobserved 3D image with the point spread function, or impulse response, of the imaging system. The PSF is the 3D response $h(x, y, z)$ of a point source of light in the system. Schlecht *et al*. [13] developed a model for the PSF of a transmitted light microscope using constraints from previous empirical observations [14]. They found that fitting it simultaneously with an independent and individual spore model improves the accuracy of detection in image stacks of *Alternaria*.

The x, y-plane in the space containing the PSF model is defined to be parallel to the focal plane, and the z-axis is aligned with the optical axis of the microscope. It is defined as a mixed function

$$\tilde{h}(x, y, z) = \frac{\alpha^{|z|}}{\sqrt{2\pi\,(\beta\,|z| + \gamma)}}\, e^{-\frac{x^2 + y^2}{2(\beta\,|z| + \gamma)}} \quad (11)$$

with $x, y \in \mathbb{R}^2$ and $z \in \mathbb{Z}$. The parameter γ is the base variance for a stack of z-axis aligned 2D Gaussians, β scales the distance from the x, y-plane, and α is the base in a geometric distribution used to weight each Gaussian.

Alternaria in the 3D image data occupy a relatively small region of the imaging window. Hence, many pixels in the data are saturated with the intensity of light used by the brightfield microscope. We define the background intensity of the imaging system over the range $[0, 1]$ and denote it as υ.

We combine the space over all PSF models and background intensities into Φ, and let a parameterization of it be an imaging model given by

$$\phi = (\alpha, \beta, \gamma, \upsilon). \quad (12)$$

3.3. Generative data model

Let $\Theta^{(\mathbf{n})} = \Psi^{(\mathbf{n})} \times \Phi$ be the parameter space over all *Alternaria* and imaging models, and let $\theta^{(\mathbf{n})} = (\psi^{(\mathbf{n})}, \phi)$ be an instance of that space. Then the solution space spanning all model configurations is

$$\Omega = \bigcup_{\mathbf{n} \in \mathbb{N}^3} \mathbf{n} \times \Theta^{(n)}. \quad (13)$$

For any $(\mathbf{n}, \theta^{(\mathbf{n})}) \in \Omega$, we generate a model scene $I_\theta(i, j, k)$, which is a hypothesis of the unobserved 3D image data. Background pixels in the model scene have the highest saturation with value υ, and pixels belonging to a substructure with opacity λ have the value $\upsilon\,(1 - \lambda)$.

Given a model scene, pixels in the 3D image data $I(i, j, k)$ are modeled as i. i. d. Gaussian with means and variances defined by

$$\mu_{I_\theta}(i, j, k) = I_\theta \ast\ast\ast \hat{h}, \quad (14)$$

$$\sigma^2_{I_\theta}(i, j, k) = c \cdot \mu_{I_\theta}(i, j, k), \quad (15)$$

where $***$ denotes 3D convolution and $\hat{h}$ is the quantized PSF model in (11).

The mean value for a pixel in $I(\cdot)$ is a weighted average of the model scene pixel intensities by the PSF model. The constant c scales the variance to approximate pixel intensity variations due to Poisson noise in the imaging system.

4. Bayesian inference

Given a stack of *Alternaria* image data $I(i,j,k)$ in the 3D window $\mathcal{W}$, we want to find the model $(\mathbf{n}, \theta^{(\mathbf{n})}) \in \Omega$ that best fits the data. We formulate this as a Bayesian statistical inference problem by defining a probability distribution over the model space given the image data and find a maximum. Specifically, we define a posterior

$$p\left(\mathbf{n}, \theta^{(\mathbf{n})} \mid I\right) = k_p \, L\left(I \mid \mathbf{n}, \theta^{(\mathbf{n})}\right) \, \pi\left(\mathbf{n}, \theta^{(\mathbf{n})}\right), \quad (16)$$

where k_p is a normalization constant, $L(\cdot \mid \cdot)$ is the likelihood of the image data, and $\pi(\cdot)$ is the model prior.

The independence assumption among pixels in the model of the image data results in a product of Gaussians for the likelihood function. Using the image model means (14) and variances (15), the likelihood is defined as

$$L\left(I \mid \mathbf{n}, \theta^{(\mathbf{n})}\right) = \prod_{i,j,k} \frac{\sigma_{I_\theta}^{-1}}{\sqrt{2\pi}} \, e^{-\frac{1}{2}\left[\frac{I(i,j,k) - \mu_{I_\theta}(i,j,k)}{\sigma_{I_\theta}}\right]^2}. \quad (17)$$

4.1. Priors

The prior over the model space Ω assumes independence between the structure and imaging models and is defined as

$$\pi\left(\mathbf{n}, \theta^{(\mathbf{n})}\right) = \pi_\Psi\left(\mathbf{n}, \psi^{(\mathbf{n})}\right) \, \pi_\Phi(\phi). \quad (18)$$

The priors for the imaging parameters ϕ are modeled as i. i. d. Gaussian. The position of the *Alternaria* root ranges uniformly over the image 3D window $\mathcal{W}$. Since the orientation and position of a substructure in *Alternaria* is determined by the configuration of its parent and its own internal parameters, we model each substructure as conditionally independent given its parent.

The density function for each substructure is composed of independent subdensities defined over its parameters. For all types of substructures, the Euler angle φ is Gaussian distributed over $[0, \pi]$, and ϑ is uniformly distributed over $[-2\pi, 2\pi]$; width w and length l are Gaussian distributed; and opacity λ is uniformly distributed over $[0, 1]$. The probability a substructure is added either laterally or apically is p_h, p_s, p_b. The lateral position d of a branch hypha is Gaussian distributed over $[0, 1]$, and the probability that a branch is created at depth t is geometrically distributed.

Let j be the index of the parent substructure of hypha h_i in $\psi^{(\mathbf{n})}$. Then the density function for hyphae is given by a set of independent subdensities

$$f_h(i \mid j) = p_h \, f_{w,l}(i \mid j) \, f_{\varphi,\vartheta}(i \mid j) f_\lambda(i \mid j). \quad (19)$$

The density functions for spores and branches are similar, but with branches having an extra term for the level t subdensity.

Finally, we restrict the interaction between substructures so they do not intersect. This is done by not allowing any of the substructures to geometrically overlap, which is not possible in the actual data. The prior probability for an *Alternaria* model is then

$$\pi_\Psi\left(\mathbf{n}, \psi^{(\mathbf{n})}\right) = k_\pi^{\mathbf{n}} \prod_{i=1}^{\mathbf{n}_h} \chi\left(h_i \nvdash h_{j \neq i}, s, b \in \psi^{(\mathbf{n})}\right) f_h\left(i \mid \mathsf{parent}(i)\right) \prod_{i=1}^{\mathbf{n}_s} \ldots \prod_{i=1}^{\mathbf{n}_b} \ldots \quad (20)$$

where $k_\pi^{\mathbf{n}}$ is a normalization constant for the truncated subdensity functions, $\vdash$ denotes geometric intersection, and $\chi(\cdot)$ is the characteristic function giving 1 for true and 0 otherwise.

5. Sampling

Inferring the most likely model given *Alternaria* image data is a challenging task; the posterior (16) is a complex distribution virtually impossible to evaluate analytically or numerically. Thus, we employ MCMC sampling to explore the model solution space in search of a maximum under the posterior [2, 11].

The sampler iteratively generates random, unbiased model samples from the solution space Ω. It consists of a set of moves, or Markov chain, that create new model proposals by proposing changes to parameters in a previous sample. The sampler moves fall into two categories: changes to *Alternaria* substructures, the PSF, or the background; and changes to the number of substructures in the model. The latter are commonly referred to as *diffusion* moves and the former *jump* moves.

At each iteration of the sampler, the m^{th} move is selected for execution with probability $r(\mathsf{m})$ and a new model $(\mathbf{n}, \tilde{\theta}^{(\mathbf{n})})$ is proposed. In this paper, we use a uniform distribution for $r(\cdot)$. Depending on how likely the new model is under the posterior and to have been proposed, it is accepted or rejected. Specifically, we use the Metropolis-Hastings (MH) algorithm for MCMC [6, 10], and it is used for both diffusion and jump moves.

5.1. Diffusion moves

The diffusion moves for modifying a substructure in $(\mathbf{n}, \theta^{(\mathbf{n})})$ and proposing a new model are rotate, resize, opacity, shift, and lateral-d. We define moves to update the PSF and background parameters, as well. The proposal distributions for diffusion moves are obtained by modifying the prior (18). For parameters updated in a move, we replace their subdensity in the prior with a Gaussian that has means equal to corresponding parameters in the previously accepted model.

For example, the proposal distribution for randomly selecting the i^{th} hypha with parent index j and rotating it is

$$q_{\mathsf{rot}}\left(\tilde{\theta}^{(\mathbf{n})} \mid \theta^{(\mathbf{n})}\right) = \frac{1}{n_h} \frac{\pi\left(\mathbf{n}, \tilde{\theta}^{(\mathbf{n})}\right)}{f_{\varphi,\vartheta}(i \mid j)} \frac{\sigma^{-2}_{\varphi,\vartheta}}{2\pi} \exp\left[-\frac{(\tilde{\varphi}_i - \varphi_i)^2 + (\tilde{\vartheta}_i - \vartheta_i)^2}{2\,\sigma^2_{\varphi,\vartheta}}\right], \quad (21)$$

where $\sigma^2_{\varphi,\vartheta}$ is a small variance. The proposal distributions for other diffusion moves are similarly constructed.

Under the MH algorithm for the rotateth diffusion move, the acceptance probability for a proposed model is

$$\alpha\left(\mathbf{n}, \tilde{\theta}^{(\mathbf{n})}\right) = \min\left\{1, \frac{p(\mathbf{n}, \tilde{\theta}^{(\mathbf{n})} \mid I)\, q_{\mathsf{rot}}(\theta^{(\mathbf{n})} \mid \tilde{\theta}^{(\mathbf{n})})}{p(\mathbf{n}, \theta^{(n)} \mid I)\, q_{\mathsf{rot}}(\tilde{\theta}^{(\mathbf{n})} \mid \theta^{(\mathbf{n})})}\right\}. \quad (22)$$

The definition is derived to maintain a detailed balance condition in the Markov chain, which is a sufficient condition for convergence to the posterior [11].

By expansion, most of the terms in (22) cancel, most notably the normalization constants and all of the non-rotation subdensities. As with the proposal distributions, the acceptance probabilities for other diffusion moves are similar; hence, their definitions are omitted.

5.2. Jump moves

The jump moves in the sampler implement model selection by changing the dimensionality of the model and accepting or rejecting. A set of birth/death moves add and remove substructures at apical or lateral positions. For apically connected hyphae and spores, merge/split moves join together or break apart two substructures. A lateral branch can be merged or split with its parent, as well. Finally, a set of switch moves transition one or more hypha to a spore and vise versa. These sampler moves embody the grammar rules for *Alternaria*.

For a hypha birth move, the proposal distribution for a new $\tilde{h}_i$ apically attached to a parent at h_j is defined as the normalized hypha density function (19) in the model prior

$$q_{\mathsf{birth}}(\tilde{h}_i \mid h_j) = k_\pi\, f_h(\tilde{i}, j\,). \quad (23)$$

During a death move, a spore is randomly selected for deletion, so a proposal distribution is not needed. The proposal distributions for merge/split and switch are similarly based on their prior subdensities.

In order to use the MH algorithm for jump moves, we redefine the acceptance probability. Following the guidelines for reversible-jump MCMC [4], the acceptance probability for a hypha birth move becomes

$$\alpha\left(\mathbf{n}+1, \tilde{\theta}^{(\mathbf{n}+1)}\right) = \min\left\{1, \frac{p(\mathbf{n}+1, \tilde{\theta}^{(\mathbf{n}+1)} \mid I)}{p(\mathbf{n}, \theta^{(\mathbf{n})} \mid I)} \frac{r(\mathsf{death})}{r(\mathsf{birth})\, q_{\mathsf{birth}}(\tilde{h}_i \mid h_j)} \left|\frac{\partial(\tilde{\theta}^{(\mathbf{n}+1)})}{\partial(\theta^{(\mathbf{n})}, \tilde{h}_i)}\right|\right\}. \quad (24)$$

Since the change in dimensionality is a one-to-one mapping from $(\tilde{h}_i, \theta^{(\mathbf{n})}) \rightarrow \tilde{\theta}^{(\mathbf{n}+1)}$ and a uniform distribution is used for $r(\cdot)$, the Jacobian is 1 and the move probabilities cancel; thus, the equation reduces considerably. Since birth/death moves are dual, the acceptance probability for a death move is the inverse of the second argument to the minimum function in (24). The acceptance probabilities for the other jump moves are similarly constructed.

As with the diffusion moves, the jump move acceptance probabilities maintain the detailed balance condition [4]. Thus, the posterior will be the stationary distribution of the trans-dimensional Markov chain followed by the sampler.

5.3. Data-driven MCMC

The spore structures in the data are much larger than the hypha and more darkly pigmented. However, we have observed that it is difficult for the sampler to correctly switch a substructure proposal from hypha to spore. Thus we improve the birth and switch moves by doing preliminary data analysis to construct a more informative proposal distribution (data-driven MCMC [18]).

The replacement proposal distribution is similar to what has been used for independent spore detection in *Alternaria* [13]. We use a gradient-based surface point detection algorithm and a very coarse Hough transform for ellipsoids to obtain rough estimates of spores in the data. The estimates are collected into a spore likelihood table, which is normalized and used as the new proposal distribution. Although the estimates from the Hough transform are very coarse, it is tolerable because diffusion moves in the sampler will perfect the fit of proposed spores.

We also used data-driven methods in the sampler to speed-up the initial estimate of the base structure in the model. We follow the assumption that the imaged growth of *Alternaria* begins at the bottom of the microscopic image stack and proceeds upward.

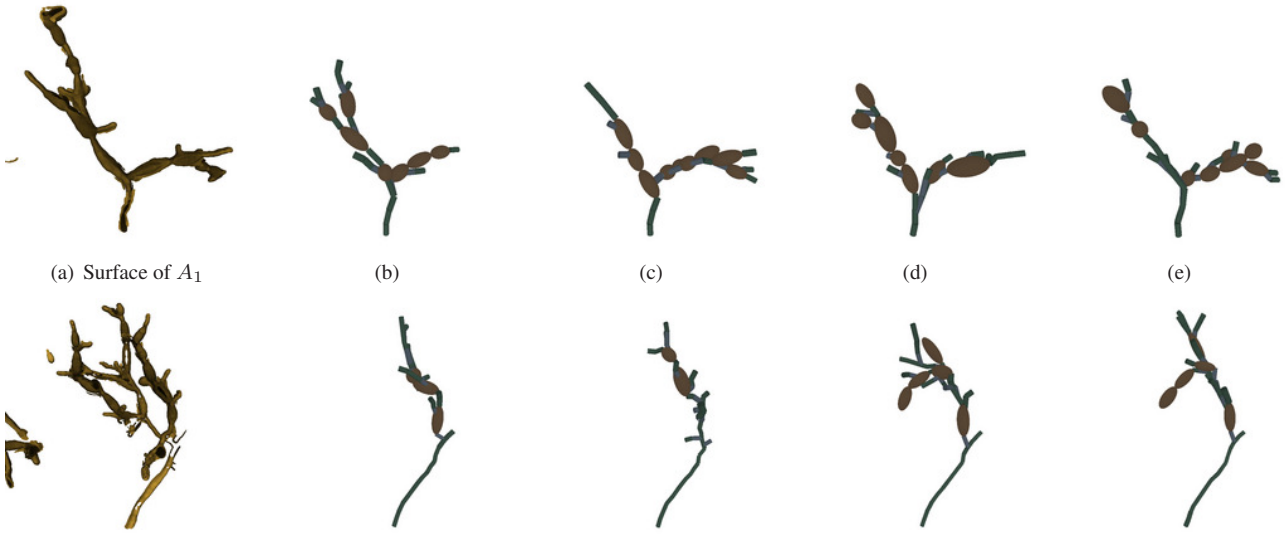

(a) Surface of A_1 (b) (c) (d) (e)

(f) Surface of A_2 (g) (h) (i) (j)

Figure 4. The sampler was run on data sets A_1 and A_2 from 10 random starting states. The first row shows a rendering of surface points from the gradient-based detection for data-driven proposals (a) from set A_1 and four of the inferred models (b)–(e). The second row shows similar results for set A_2 (f)–(j). We are clearly fitting *Alternaria* structure in the data. If we continue to run the sampler, more of the structure would be fit, particularly in the case of A_2.

6. Results

We evaluated the effectiveness of the model sampler on *Alternaria* image sets A_1 and A_2, shown in figure 1. A_1 is composed of 102 images of size 800×800 pixels and A_2 has 82 images of size 700×700. Since the data are so large, we down-sample them along rows and columns to 20% of their original size. However, since the number of images in each stack is already disproportionately small, we did not decrease the resolution in depth.

We ran the sampler from 10 random starting states on both data sets, each for $20,000$ iterations. Figure 4 shows four of the ten models fit to each data set. The sampler had a more difficult time fitting the structure in A_2; a narrow lateral hypha spawned very large areas of structure. With more iterations we would expect to begin to fit more of it.

The average inferred background intensity for A_1 and A_2 was 0.74 and 0.72 with a negligible standard deviation. Table 1 gives the inferred PSF model parameters for the data sets. The PSF parameters for A_2 have larger variance because not as much structure was fit in the images as A_1.

Figure 5 shows two images from A_1 at different depths compared to corresponding inferred model scene images. We construct the model scene images by optically sectioning the *Alternaria* model and convolving it with the point-spread function. From these images we observe that simultaneously fitting structure and imaging models closely resembles the image formation process, enabling us to obtain a more accurate fit to the data.

	α		β		γ	
	mean	stdev	mean	stdev	mean	stdev
A_1	0.99	0.001	0.91	0.08	0.75	0.26
A_2	0.84	0.14	0.68	0.4	0.64	0.24

Table 1. Mean PSF model parameters inferred from the *Alternaria* data from 10 random starting states. The larger variance in the parameters for the second set is most likely from not fitting as much structure.

7. Conclusion

Learning the structure of an object is one of the first steps in trying to understand its function. Biologists recognize this fact and conduct many experiments that require analyzing images of microscopic structures. We have shown that combining a grammar-based specimen model with an imaging model is useful to automatically obtain quantitative information for biological structures in microscopic image stacks.

References

[1] F. Al-Awadhi, C. Jennison, and M. Hurn. Statistical image analysis for a confocal microscopy two-dimensional section of cartilage growth. *Journal of the Royal Statistical Society: Applied Statistics*, 53(1):31–49, 2004.

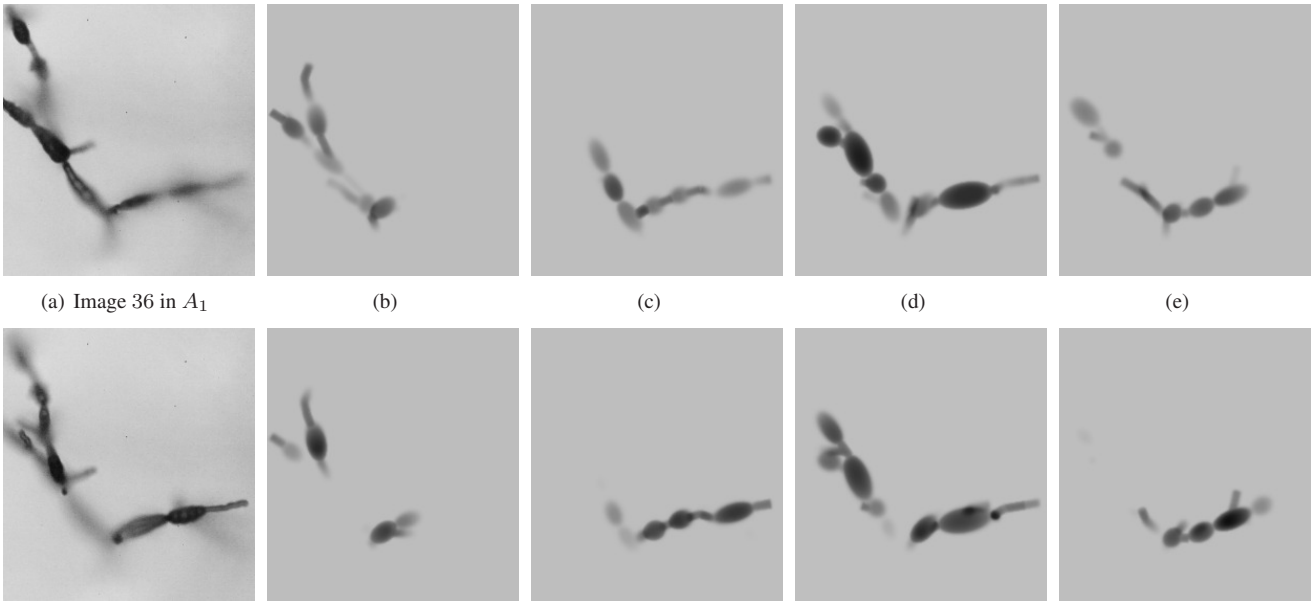

(a) Image 36 in A_1 (b) (c) (d) (e)

(f) Image 48 in A_1 (g) (h) (i) (j)

Figure 5. Simultaneously modeling the structure and imaging system more accurately explains blurred microscopic images. Row one shows image 36 of A_1 compared with images at the same depth from the inferred model scenes. Image 48 in the stack is shown in the second row. The generated model scene is the optically sectioned images of a fit *Alternaria* and imaging system. Each column shows images generated by the model for A_1 corresponding to the same column of figure 4, *e.g.*, images 5(b) and 5(g) are from the model in figure 4(b). The model scene images for A_2 have similar results.

[2] C. Andrieu, N. de Freitas, A. Doucet, and M. I. Jordan. An introduction to MCMC for machine learning. *Machine Learning*, 50(1):5–43, 2003.

[3] J. Conchello. Superresolution and convergence properties of the expectation-maximization algorithm for maximum-likelihood deconvolution of incoherent images. *Journal of Optical Society of America A*, 15(10):2609–2619, 1998.

[4] P. J. Green. Reversible jump Markov chain Monte Carlo computation and Bayesian model determination. *Biometrika*, 82(4):711–732, 1995.

[5] L. Gui-ting, Q. Yu-zhen, Z. Peng, D. Wei-hua, Q. Yuan-ming, and G. Hong-tao. Etiological role of *alternaria* alternata in human esophageal cancer. *Chin Medical Journal*, 105(5):394–400, 1992.

[6] W. K. Hastings. Monte Carlo sampling methods using Markov chains and their applications. *Biometrika*, 57:97–109, 1970.

[7] T. J. Holmes. Blind deconvolution of quantum-limited incoherent imagery: maximum-likelihood approach. *Journal of Optical Society of America A*, 9:1052–1061, 1992.

[8] A. Lindenmayer. Mathematical models for cellular interaction in development, parts i and ii. *Journal of Theoretical Biology*, 18(3):280–299, 300–315, 1968.

[9] A. Lindenmayer. Developmental algorithms for multicellular organisms: A survey of L-systems. *Journal of Theoretical Biology*, 54(1):3–22, 1975.

[10] N. Metropolis, A. W. Rosenbluth, M. N. Rosenbluth, A. H. Teller, and E. Teller. Equations of state calculations by fast computing machines. *Journal of Chemical Physics*, 21:1087–1092, 1953.

[11] R. M. Neal. Probabilistic inference using Markov chain Monte Carlo methods. Technical Report CRG-TR-93-1, University of Toronto, 1993.

[12] P. Prusinkiewicz, A. Lindenmayer, and J. Hanan, editors. *The algorithmic beauty of plants*. Springer-Verlag, 1990.

[13] J. Schlecht, K. Barnard, and B. Pryor. Statistical inference of biological structure and point spread functions in 3D microscopy. In *Proceedings of the Third International Symposium on 3D Data Processing, Visualization and Transmission*, June 2006.

[14] P. J. Shaw and D. J. Rawlins. The point-spread function of a confocal microscope: its measurement and use in deconvolution of 3-d data. *Journal of Microscopy*, 163(2):151–165, 1991.

[15] E. Simmons. Alternaria themes and variations (287-304): Species on caryophyllaceae. *Mycotaxon*, 70:325–369, 1999.

[16] K. Wilken-Jensen and S. Gravesen. *Atlas of moulds in Europe causing respiratory allergy*. ASK Publishing, Copenhagen, Denmark, 1984.

[17] C. Wilson and M. Wisniewski. *Biological control of postharvest diseases: theory and practice*. CRC Press Inc., Boca Raton, Fla., 1994.

[18] S.-C. Zhu, R. Zhang, and Z. Tu. Integrating top-down/bottom-up for object recognition by data driven Markov chain Monte Carlo. In *Computer Vision and Pattern Recognition*, 2000.